Vítor Monteiro, Bruno Exposto, J. G. Pinto, M. J. Sepúlveda, Andrés A. Nogueiras Meléndez, João L. Afonso

"Three-Phase Three-Level Current-Source Converter for EVs Fast Battery Charging Systems"

IEEE ICIT International Conference on Industrial Technology, Seville Spain, pp.1401-1406, March 2015.

http://ieeexplore.ieee.org/stamp/stamp.jsp?tp=&arnumber=7125293

ISBN: 978-1-4799-7799-4

DOI: 10.1109/ICIT.2015.7125293

Vítor Monteiro, Bruno Exposto, J. G. Pinto, M. J. Sepúlveda, Andrés A. Nogueiras Meléndez, João L. Afonso, "Three-Phase Three-Level Current-Source Converter for EVs Fast Battery Charging Systems," IEEE ICIT International Conference on Industrial Technology, Seville Spain, pp.1401-1406, March 2015. DOI: 10.1109/ICIT.2015.7125293, ISBN: 978-1-4799-7799-4

Three-Phase Three-Level Current-Source Converter for EVs Fast Battery Charging Systems

Vítor Monteiro[1], Bruno Exposto[1], J. G. Pinto[1], M. J. Sepúlveda[1], Andrés A. Nogueiras Meléndez[2], João L. Afonso[1]
[1]ALGORITMI Research Centre – University of Minho, Guimarães – Portugal
[2]Departamento de Tecnología Electrónica – University of Vigo, Vigo – Spain
[1]{vitor.monteiro | bruno.exposto | gabriel.pinto | sepulveda.freitas | joao.l.afonso}@algoritmi.uminho.pt [2]aaugusto@uvigo.es

***Abstract*—This paper presents a three-phase three-level fast battery charger for electric vehicles (EVs) based in a current-source converter (CSC). Compared with the traditional voltage-source converters used for fast battery chargers, the CSC can be seen as a natural buck-type converter, i.e., the output voltage can assume a wide range of values, which varies between zero and the maximum instantaneous value of the power grid phase-to-phase voltage. Moreover, using the CSC it is not necessary to use a dc-dc back-end converter in the battery side, and it is also possible to control the grid current in order to obtain a sinusoidal waveform, and in phase with the power grid voltage (unitary power factor). Along the paper is described in detail the proposed CSC for EVs fast battery charging systems: the circuit topology, the power control theory, the current control strategy and the grid synchronization algorithm. Several simulation results of the EV fast battery charger operating with a maximum power of 50 kW are presented.**

Keywords—Electric Vehicle; Current-Source Converter; Fast Battery Charger.

I. INTRODUCTION

The growing interest of electric mobility contributes to the migration to a new paradigm in the transport sector and to a more sustainable and efficient mobility [1][2]. For instance, in [3] is presented a comparison of an electric vehicle (EV) and a diesel powered vehicle in terms of energy consumption, and is concluded that the EV is significantly more energy efficient than the diesel vehicle in a tank-to-wheel perspective. As presented in [4], with the electric mobility paradigm, emerges several opportunities and challenges for the EVs integration in the power grids. However, this new paradigm will only be viable if the EVs have competitive costs, both production, purchasing and maintenance, as well as effective control strategies for its integration in the power grids [5][6]. Alongside with this, the time required to perform the EV battery charging process is one of the main issues that must be addressed by the EVs battery chargers [7][8]. Nowadays, to mitigate this issue are used public fast battery chargers with an operating power above 50 kW [9]. However, considering that a great amount of power is delivered in such a short time, it is possible identify advantages and disadvantages when this method is compared with slow battery chargers [10]. Taking into account that the required energy is provided from the power grid it is expected that the power quality issues are not neglected [11][12][13]. The EV battery charging process requires the conversion of ac voltage from the power grid to a dc voltage to charge the batteries. This conversion is done by ac-dc power electronics converters, which can be designed with a single stage (ac-dc front-end converter) or with a double stage (ac-dc front-end and a dc-dc back-end converters). The ac-dc front-end converters of the fast battery chargers can be designed with passive or active power converters [14][15]. The main passive power converters are the full-bridge diode rectifier and the multi-pulse rectifiers, where are used transformers with several windings connected in specific configurations aiming to reduce the harmonic content of the main current [16][17]. Although its simplicity, these power converters are not the most appropriated converters for EV fast battery chargers, once it is not possible reduce drastically the harmonic content of the grid current and are heavy and bulky. On the other hand, the main active power converters are based, for instance, in the full-bridge full-controlled converter, the SWISS and VIENNA converters, and the neutral-point-clamped converter [18][19]. Although the complexity of the active power converters, they are the most appropriated for fast battery chargers, once it is possible regulate the dc-link voltage and minimize the grid current harmonic content. The aforementioned active power converters are boost-type voltage-source converters controlled by current, where the dc-link voltage is greater than the power grid voltage maximum value. Therefore, it is required use a buck-type dc-dc back-end converter to adjust the dc-link voltage to an appropriated level to charge the EV batteries.

Fig. 1 shows the circuit topology of the proposed EV fast battery charger based in a current-source converter (CSC). As it can be seen, instead of using capacitors in the dc side, it is used an inductor as energy storage element. In order to ensure the proper operation as active rectifier, i.e., with sinusoidal current and unitary power factor in the ac side, it is required the use of a LC filter in the ac side. Although there are galvanically isolated solutions [9], the proposed topology is non isolated, once the isolation only should be guaranteed between the traction batteries and the auxiliary battery. Taking into account that the presented topology is a current source type, the dc link current cannot be interrupted. Therefore, the EV connection or

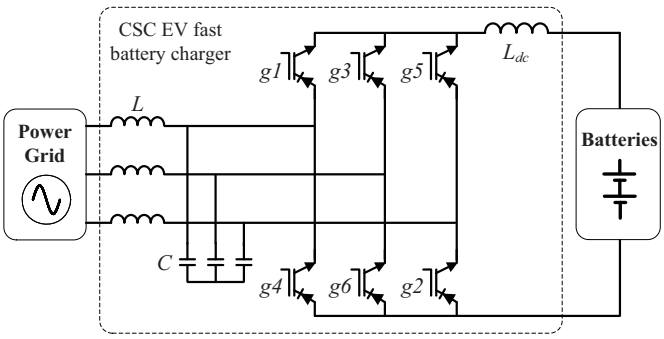

Fig. 1. Circuit topology of the EV fast battery charger based in a CSC.

disconnection to the converter is only performed when the dc link current is zero. In [20] is presented a CSC used as a motor drive in EVs, and that is combined with a V-I converter to interface the dc-link (current) and the batteries (voltage). In this application, the V-I converter is used to charge or discharge the batteries. Nevertheless, using a single CSC between the power grid and the batteries, it is possible avoid the use of the dc-dc back-end converter due to CSC capability to operate as buck converter. Moreover, CSC operates as active rectifier allowing sinusoidal current and unitary power factor in the ac side [21][22]. These main advantages of the CSC allow reduce the total cost and volume in applications as EV fast battery chargers. Therefore, this paper presents a three-phase three-level CSC for EV fast battery chargers. The rest of this paper is structured as follows. In section II is presented the CSC fast battery charger principle of operation, where are included the main specifications and the synchronism with the power grid voltage. In section III is presented the CSC controller design, namely, the power theory and the current control strategy. In section IV are presented the main simulation results, where the EV fast battery charger operates with a maximum power of 50 kW. Finally, section V presents the main conclusions.

II. CSC Fast Battery Charger Description

The converter presented in this paper to perform the EV fast battery charging is composed by a single ac-dc front-end converter, which is based in a three-phase three-level CSC. Table I shows the main specifications of the proposed CSC EV fast battery charger. These specifications were selected aiming to be possible to perform a traditional EV fast battery charging process. As example, in [23] is presented the charging profile of a *Nissan Leaf* during approximately 30 minutes until the battery state-of-charge reaches 80%. Fig. 2 shows the current and power measured during a charging cycle. In order to obtain sinusoidal currents and almost unitary power factor, it is mandatory that the CSC controller must be synchronized with the positive sequence of the power grid fundamental voltage. In the scope of this paper was used the three-phase phase-locked loop implemented in $\alpha\beta$ coordinates ($\alpha\beta$-PLL) proposed in [24], in order to track the positive sequence component at the fundamental frequency. Fig. 3 shows the algorithm of this $\alpha\beta$-PLL. As it can be seen, the feedback signals pll_α and pll_β result from the calculation of the sine and co-sine of ωt, which represents the output angle given by the integrator. These signals have unitary amplitude and correspond to the direct and quadrature components of the positive sequence of the fundamental power grid voltages. The $\alpha\beta$-PLL is the first algorithm implemented by the CSC controller, once it is used as input to the subsequent control algorithms.

III. CSC Controller Design

In this section is presented the CSC controller design, namely, the power theory that allows define the grid current references in function of the battery charging current, and the current control strategy that allows the CSC to synthetize the current references. Fig. 4 shows the single-phase equivalent circuit of the EV fast battery charger, where are represented the main currents and voltages, for both ac and dc side. This equivalent circuit is used to describe the circuit equations in a simple way.

TABLE I
CSC EV FAST BATTERY CHARGER SPECIFICATIONS.

Parameters	Value	Unit
Grid Voltage (line-to-neutral)	230 ± 10%	V
Grid Frequency	50 ± 1%	Hz
Maximum Input Power	50	kVA
$THD\%_v$	< 8%	
$THD\%_i$ @ Full Load	< 1%	
Total Power Factor @ Full Load	0.99	
Switching Frequency	20	kHz
Output dc Voltage Range	0 to 500	V
Maximum Output Current	120	A
Maximum Output Power	50	kW
Input Inductor L	500	µH
Damping Resistor	10	Ω
Input Capacitor C	200	µF
Output Inductor L_{dc}	20	mH

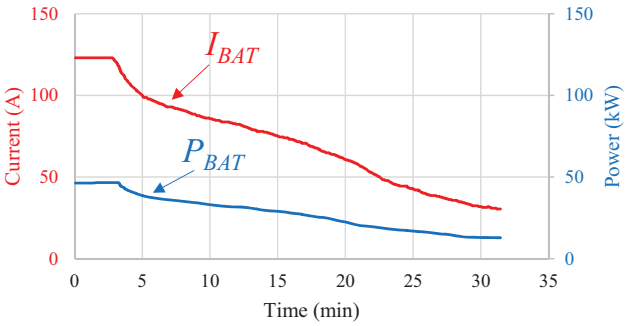

Fig. 2. Fast charging profile of a *Nissan Leaf* (according with [23]).

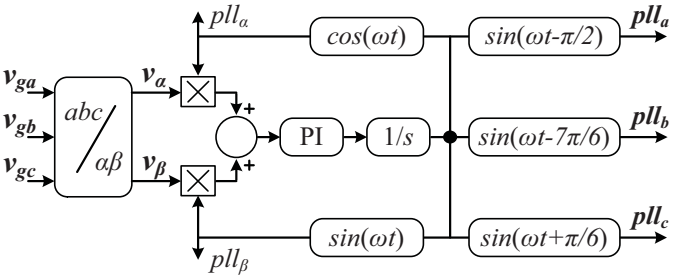

Fig. 3. Block diagram of the three-phase $\alpha\beta$-PLL algorithm.

A. Power Theory

In this item is presented the power theory beyond the CSC control algorithm. In order to simplify the power theory description, in this item is assumed that the power grid voltage is composed only by the fundamental component. However, in the CSC digital controller is used an $\alpha\beta$-PLL, allowing to obtain sinusoidal references to the grid current. Considering that the single-phase power grid voltage (v_g) and the single-phase grid current (i_g) are expressed, respectively, by:

$$v_g = \sqrt{2}\ V_g\ sen\ (\omega t)\,, \tag{1}$$

$$i_g = \sqrt{2}\ I_g\ sen\ (\omega t + \varphi)\,, \tag{2}$$

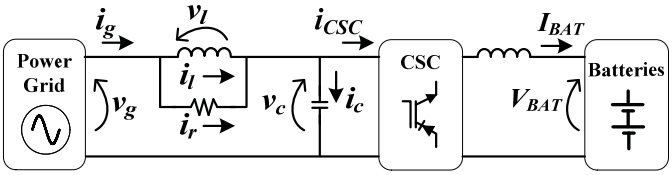

Fig. 4. Single-phase equivalent circuit of the EV fast battery charger.

the three-phase active power (P_g) in the ac side can be defined by:

$$P_g = V_{ga}\, I_{ga} \cos(\varphi_a) + V_{gb}\, I_{gb} \cos(\varphi_b) + \\ + V_{gc}\, I_{gc} \cos(\varphi_c)\,. \tag{3}$$

Considering that is only transferred active power from the power grid to the batteries, the power grid voltage (v_g) and the grid current (i_g) are in phase, i.e., φ=0. Therefore, from (3) it can be defined an equivalent single-phase conductance (G), seen from the CSC output according to:

$$G = \frac{P_g}{3\, {V_g}^2}\,, \tag{4}$$

where, V_g corresponds to the rms value of each single-phase power grid voltage (v_{ga}, v_{gb}, and v_{gc}). Using the conductance defined in (4), the single-phase instantaneous grid current reference for each phase can be defined by:

$${i_g}^* = G\; pll\; \sqrt{2}\, V_g\,, \tag{5}$$

where, *pll* is the output of the three-phase $\alpha\beta$-PLL algorithm and can assume the values of pll_a, pll_b or pll_c, according to the power grid phase. It is important to refer that using this strategy, the grid currents (i_{ga}, i_{gb}, and i_{gc}) will be sinusoidal even under power grid voltages (v_{ga}, v_{gb}, and v_{gc}) with high harmonic content. It is important to refer that using this strategy, the grid currents (i_{ga}, i_{gb}, and i_{gc}) will be balanced even under unbalance voltages (v_{ga}, v_{gb}, and v_{gc}). Neglecting the CSC losses, the active power P_g corresponds to the power to charge the batteries. Therefore, substituting (4) in (5) is obtained:

$${i_g}^* = \frac{P_{BAT}}{3\, {V_g}^2}\; pll\; \sqrt{2}\, V_g\,. \tag{6}$$

Substituting P_{BAT} is obtained:

$${i_g}^* = \frac{V_{BAT}\; I_{BAT}}{3\, {V_g}^2}\; pll\; \sqrt{2}\, V_g\,, \tag{7}$$

where, I_{BAT} is the current in the dc-link and is controlled by a PI controller.

B. Current Control Theory

From Fig. 4, analyzing the voltages and currents between the power grid and the CSC, it can be established that:

$$i_g = i_r + i_l = i_c + i_{CSC}\,, \tag{8}$$

$$v_g = v_l + v_c\,. \tag{9}$$

Taking into account that $i_r \ll i_l$, it can be assumed that $i_g \approx i_l$ without introduce significant error to the circuit analysis. Substituting the current in the capacitor (i_c) represented in (8) by the time derivative of its voltage multiplied by its capacitance, it can be established:

$$i_g = \mathrm{C}\frac{dv_c}{dt} + i_{CSC}\,. \tag{10}$$

Substituting (9) in (10) and rearranging in order to the current (i_{CSC}) that the CSC must produce is obtained:

$$i_{CSC} = i_g - C\,\frac{dv_g}{dt} + C\,\frac{dv_l}{dt}\,. \tag{11}$$

Finally, substituting the voltage in the inductor (v_l) by the time derivative of its current multiplied by its inductance, it can be established:

$$i_{CSC} = i_g - \mathrm{C}\frac{dv_g}{dt} + \mathrm{CL}\frac{d^2 i_g}{dt^2}\,. \tag{12}$$

Taking into account that is used a digital control system, the derivative of the power grid voltage (v_g) in (12) can be substituted by its discrete implementation using the forward Euler method according to:

$$\frac{dv_g}{dt} = \frac{v_g[k+1] - v_g[k]}{T_s}\,, \tag{13}$$

and the second order derivative of the power grid current in (12) can be substituted by its discrete implementation defined as:

$$\frac{d^2 i_g}{dt^2} = \frac{i_g[k+1] - 2i_g[k] + i_g[k-1]}{{T_s}^2}\,, \tag{14}$$

Using (13) and (14), the discrete implementation of (12) results in:

$$i_{CSC}[k] = i_g[\mathrm{k}] - \mathrm{C}f_s(v_g[k+1] - v_g[k]) + \\ + \mathrm{CL}{f_s}^2\big(i_g[k+1] - 2i_g[k] + i_g[k-1]\big)\,, \tag{15}$$

where, f_s is the sampling frequency, and *k*, *k-1*, *k+1*, are respectively, the actual, previous and next samples. The purpose of this control law is make the error between the grid current (i_g) and its reference (i_g*) at instant *k* equal to zero at time *k+1*. Therefore, (15) can be rewritten for:

$$i_{CSC}[k] = i_g[\mathrm{k}] - \mathrm{C}f_s(v_g[k+1] - v_g[k]) + \\ + \mathrm{CL}{f_s}^2\big({i_g}^*[k] - 2i_g[k] + i_g[k-1]\big)\,. \tag{16}$$

In order to compute (16) is necessary know the value of the power grid voltage (v_g) in the instant *k+1*. This value can be obtained from the present and previous values using a Lagrange extrapolation [25] given by:

$$v_g[k+1] = 3v_g[k] - 3v_g[k-1] + v_g[k-2]\,. \tag{17}$$

Substituting (17) in (16) is obtained the final current control law that allows control the current produced by the CSC. The current $i_{CSC}[k]$ is the reference that is used to control the state of the CSC switches. The gate pulse patterns that allow synthesize this current are obtained from a combinational logic circuit [26], which is responsible to generate the CSC valid states, as presented in table II. The input of the combinational logic circuit is the result of the comparison between the current $i_{CSC}[k]$ and a pulse-width modulator (PWM) with 20 kHz center-aligned triangular carrier.

IV. Simulation Results

In this item are presented some simulation results obtained during the EV fast battery charging process under the conditions of phase-to-phase power grid voltage of 400 V, and with a maximum charging power of 50 kW. The simulation results were obtained with the simulation software PSIM 9.0, where is included the hardware topology, the digital control system, and the battery model. It is important to refer that the simulation mode of the CSC uses IGBTs as controlled semiconductors in series with diodes (once IGBTs do not have reverse-blocking capability). However, in a perspective of a future practical implementation, it can be considered use RB-IGBTs as suggested in Fig. 1. In the simulations were considered lithium ion batteries with a nominal voltage of 360 V and with a nominal energy of 20 kWh. Although the EV battery charger was mainly designed to charge lithium batteries, it can be used to charge any type of batteries. In order to prevent resonance due to the LC filter, it was used a damping resistor of 10 Ω in parallel with the L filter. Taking into account the aforementioned CSC controller design, during all the process of the EV fast battery charging, the grid current (i_g) is sinusoidal and in phase with the power grid voltage (v_g). In the scope of this paper, it is assumed that the power grid voltage has a total harmonic distortion of about 2%.

For the phase *a*, Fig. 5 (a) shows the power grid voltage (v_{ga}) and the grid current (i_{ga}). Fig. 5 (b) shows in detail when the power grid voltage (v_{ga}) and the grid current (i_{ga}) crosses zero. Fig. 5 (c) shows in detail the grid current (i_{ga}) ripple. These simulation results were obtained with a power of 50 kW and a measured total power factor of 0.99. As show in Fig. 5, due to the power theory (cf. section III A) and the grid current control strategy (cf. section III B), the grid current (i_{ga}) is sinusoidal with low harmonic distortion. However, taking into account that the charging power varies during the battery charging process (Fig. 2), the grid current THD% also varies. Fig. 6 shows the grid current THD% in function of the charging power (with a variation between 10 kW and 50 kW). Once the power grid voltage has harmonic content (about of 2%), and since it is used a PLL (cf. section II) in the power theory, the grid current does not vary linearly with the power grid voltage. Fig. 7 shows the power grid voltage (v_g) in function of the grid current (i_g). As it can be seen, the variation is approximately linear between -75 A and 75 A, and is much nonlinear near of the maximum values (i.e., above ±100 A and ±300 V). This situation occurs because the power grid voltages waveform is not purely sinusoidal (it presents a THD% of about 2%). Fig. 8 shows the instantaneous value of the grid current error in function of the grid current (i_g) during the charging process with a power (P_{BAT}) of 50 kW. As it can be seen, the maximum current error occurs near of the maximum value (±100 A) and the maximum current error is below 2 A.

For the phase *a*, Fig. 9 shows the grid current (i_{ga}), the current in the input capacitor (i_c), the current produced by the CSC (i_{CSCa}), and the current in the dc-link (I_{BAT}). As it can be seen, the grid current (i_g) is sinusoidal, the dc-link current (I_{BAT}) is maintained constant with a value of 120 A (that corresponds to a current for the maximum power of the battery charging process) with low current ripple, the current produced by the CSC (i_{CSCa}) has three-levels ($-I_{BAT}$, *0*, $+I_{BAT}$), and the current in the input capacitor (i_c) is in accordance with the CSC current in order to maintain the grid current (i_g) sinusoidal and in phase with the power grid voltage (v_g). Fig. 10 shows the phase to neutral power grid voltages (v_{ga}, v_{gb}, and v_{gc}), the grid currents (i_{ga}, i_{gb}, and i_{gc}), and the current produced by the CSC (i_{CSCa}) in phase *a*.

Fig. 11 shows some simulation results related with the dc-link current (I_{BAT}). Fig. 11 (a) shows the dc-link current (I_{BAT}) during a complete EV fast battery charging process. The

TABLE II
CSC VALID STATES.

g1	*g4*	*g3*	*g6*	*g5*	*g2*	i_{CSCa}	i_{CSCb}	i_{CSCc}
1	0	0	0	0	1	$+I_{BAT}$	*0*	$-I_{BAT}$
0	0	1	0	0	1	*0*	$+I_{BAT}$	$-I_{BAT}$
0	1	1	0	0	0	$-I_{BAT}$	$+I_{BAT}$	*0*
0	1	0	0	1	0	$-I_{BAT}$	*0*	$+I_{BAT}$
0	0	0	1	1	0	*0*	$-I_{BAT}$	$+I_{BAT}$
1	0	0	1	0	0	$+I_{BAT}$	$-I_{BAT}$	*0*
1	1	0	0	0	0	*0*	*0*	*0*
0	0	1	1	0	0	*0*	*0*	*0*
0	0	0	0	1	1	*0*	*0*	*0*

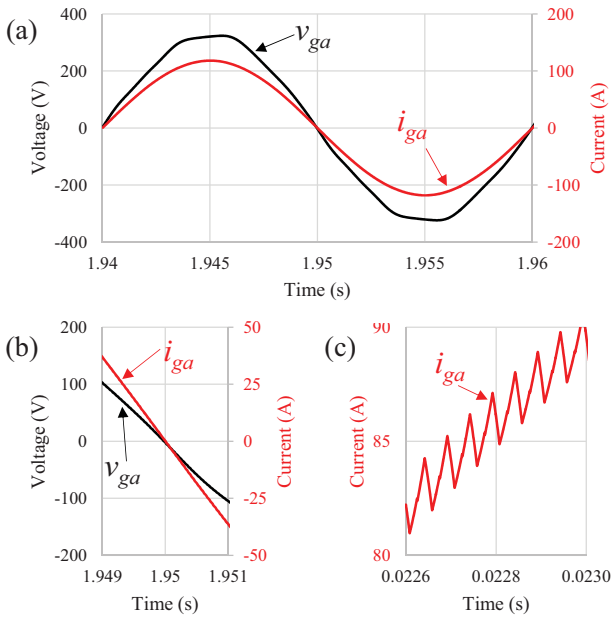

Fig. 5. Simulation results during the EV fast battery charging process: (a) Waveforms of the power grid voltage (v_{ga}) and grid current (i_{ga}) during 20 ms; (b) Detail of the power grid voltage (v_{ga}) and grid current (i_{ga}) crossing zero; (c) Detail of the grid current (i_{ga}) ripple.

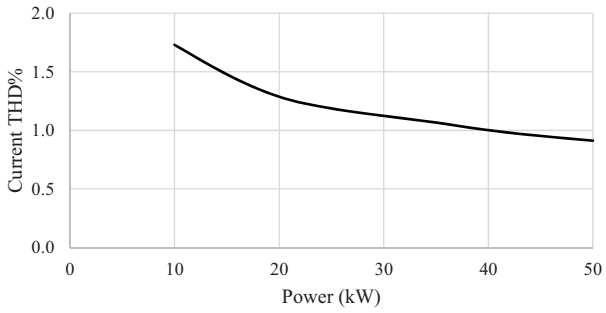

Fig. 6. Grid current (i_g) THD% in relation to the EV charging power.

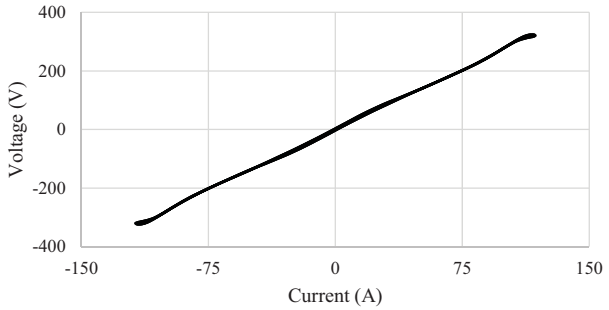

Fig. 7. Power grid voltage (v_g) in function of the grid current (i_g).

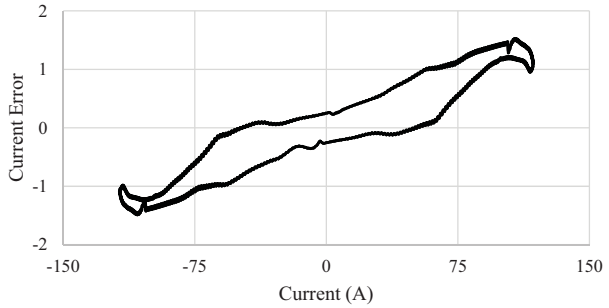

Fig. 8. Grid current error in function of the grid current (i_g) during the charging process with a power (P_{BAT}) of 50 kW.

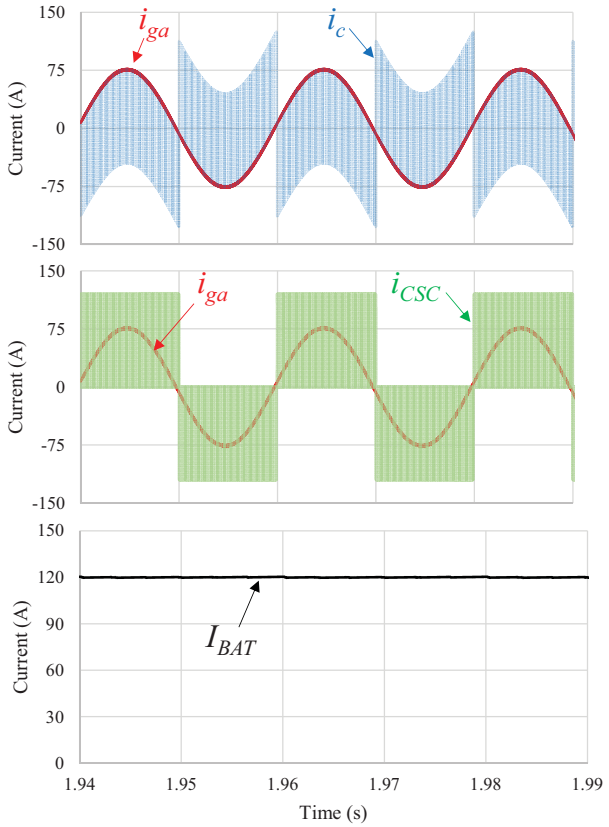

Fig. 9. Grid current (i_{ga}), current produced by the CSC (i_{CSCa}), current in the input capacitor (i_c), and current in the dc-link (I_{BAT}), during the EV fast charging process with a power (P_{BAT}) of 50 kW.

charging process starts with a current value of 120 A during almost 4 minutes. The battery charging process is interrupted when the battery state-of-charge reaches 80%. This situation occurs when the charging current decreases to 30 A. The time

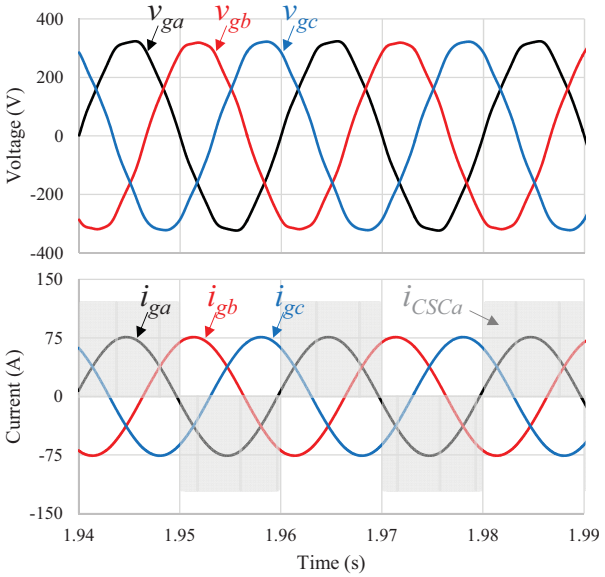

Fig. 10. Power grid voltages (v_{ga}, v_{gb}, and v_{gc}), grid currents (i_{ga}, i_{gb}, and i_{gc}), and current produced by the CSC (i_{CSCa}) in phase *a*.

required to perform the battery charging was 30 minutes. Fig. 11 (b) shows the dc-link current (I_{BAT}) ripple during a time interval of 100 ms. Fig. 11 (c) shows the dc-link current (I_{BAT}) in function of the line current (i_{ga}).

V. Conclusions

This paper presents an EV fast battery charger based in a three-phase three-level CSC. Taking into account that the CSC is a natural buck-type converter, it can be used instead of voltage-source converters, mainly because it is not required the use of a dc-dc back-end converter. Therefore, the output voltage can assume a wide range of values (between zero and the maximum instantaneous value of the phase-to-phase power grid voltage). Besides this advantage, the CSC can also be used to maintain the grid current with a sinusoidal waveform, and in phase with the power grid voltage (unitary power factor), contributing to preserve the power quality of the electrical power grid. Moreover, due to the CSC control algorithm (power theory and current control strategy), which allows to obtain sinusoidal current references (using the PLL signals), the grid currents present sinusoidal waveform, even with distorted power grid voltages (the voltages present a THD% of about 2%). The CSC power theory and the current control strategy, as well as the CSC grid synchronization, are presented along the paper. In order to attest the feasibility of the CSC operating as fast battery charger are presented several simulation results for operation with a maximum power of 50 kW.

Acknowledgment

This work has been supported by FCT – Fundação para a Ciência e Tecnologia within the Project Scope: UID/CEC/00319/2013. Mr. Vítor Monteiro was supported by the doctoral scholarship SFRH/BD/80155/2011 granted by the FCT agency.

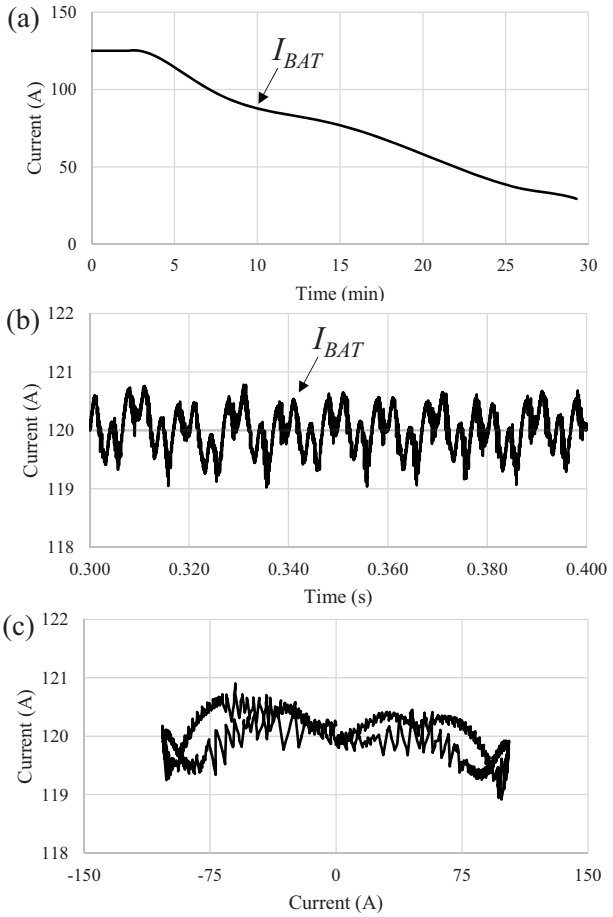

Fig. 11. Simulation results of: (a) Dc-link current (I_{BAT}) during the EV fast battery charging process in a time interval of 30 minutes; (b) Dc-link current (I_{BAT}) ripple during in a time interval of 100 ms; (c) Dc-link current (I_{BAT}) in function of the line current (i_{ga}).

REFERENCES

[1] Kaushik Rajashekara, "Present Status and Future Trends in Electric Vehicle Propulsion Technologies," IEEE J. Emerg. Sel. Topics Power Electron., vol.1, no.1, pp.3-10, Mar. 2013.

[2] Thomas H. Bradley, Andrew A. Frank, "Design, demonstrations and sustainability impact assessments for plug-in hybrid electric vehicles," ELSEVIER Renewable and Sustainable Energy Reviews, pp.1-14, May 2007. .

[3] J. Martins, F. P. Brito, D. Pedrosa, Vítor Monteiro, João L. Afonso, "Real-Life Comparison between Diesel and Electric Car Energy Consumption," in Grid Electrified Vehicles: Performance, Design and Environmental Impacts, 1st ed., Carla Alexandra Monteiro da Silva, Ed. Nova Science Publishers, 2013, Chapter 10, pp.209-232. .

[4] Chunhua Liu, K. T. Chau, Diyun Wu, Shuang Gao, "Opportunities and Challenges of Vehicle-to-Home, Vehicle-to-Vehicle, and Vehicle-to-Grid Technologies," Proc. IEEE, vol.101, no.11, pp.2409-2427, Nov. 2013.

[5] João C. Ferreira, Vitor Monteiro, João L. Afonso, "Vehicle-to-Anything Application (V2Anything App) for Electric Vehicles," IEEE Trans. Ind. Informat., vol.10, no.3, pp.1927-1937, Aug. 2014.

[6] Farzad Rajaei Salmasi, "Control Strategies for Hybrid Electric Vehicles: Evolution, Classification, Comparison, and Future Trends," IEEE Trans. Veh. Technol., vol.56, no.5, pp.2393-2404, Sept. 2007.

[7] Shyh-Jier Huang, Bo-Ge Huang, Fu-Sheng Pai, "Fast Charge Strategy Based on the Characterization and Evaluation of LiFePO4 Batteries," IEEE Trans. Power Electron., vol.28, no.4, pp.1555-1562, Apr. 2013.

[8] Deepak S. Gautam, Fariborz Musavi, Murray Edington, Wilson Eberle, William G. Dunford, "An Automotive Onboard 3.3-kW Battery Charger for PHEV Application," IEEE Trans. Veh. Technol., vol.61, no.8, pp.3466-3474, Oct. 2012.

[9] D. Aggeler, F. Canales, H. Zelaya - De La Parra, A. Coccia, N. Butcher, O. Apeldoorn, "Ultra-Fast DC-Charge Infrastructures for EV-Mobility and Future Smart Grids," IEEE Innovative Smart Grid Technologies Conference Europe, pp.1-8, Oct. 2010.

[10] Charles Botsford, Adam Szczepanek, "Fast Charging vs. Slow Charging: Pros and Cons for the New Age of Electric Vehicles," EVS24 International Battery, Hybrid and Fuel Cell Electric Vehicle Symposium, pp.1-9, May 2009.

[11] J. G. Pinto, Vítor Monteiro, Henrique Gonçalves, João L. Afonso, "Onboard Reconfigurable Battery Charger for ElectricVehiclesWith Traction-to-Auxiliary Mode," IEEE Trans. Veh. Technol., vol.63, no.3, pp.1104-1116, Mar. 2014.

[12] Vítor Monteiro, Henrique Gonçalves, João L. Afonso, "Impact of Electric Vehicles on Power Quality in a Smart Grid Context," IEEE EPQU International Conference on Electrical Power Quality and Utilisation, pp.1-6, Oct. 2011.

[13] J. Carlos Gómez, Medhat M. Morcos, "Impact of EV Battery Chargers on the Power Quality of Distribution Systems," IEEE Trans. Power Del., vol.18, no.3, pp. 975-981, July 2003.

[14] Sanzhong Bai, Srdjan M. Lukic, "Unified Active Filter and Energy Storage System for an MWElectric Vehicle Charging Station," IEEE Trans. Power Electron., vol.28, no.12, pp.5793-5803, Dec. 2013.

[15] T. Soeiro, T. Friedli, J. W. Kolar, "Three-Phase High Power Factor Mains Interface Concepts for Electric Vehicle Battery Charging Systems," IEEE APEC Applied Power Electronics Conference and Exposition, pp.2603-2610, Feb. 2012.

[16] Derek A. Paice, "Power Electronics Converter Harmonics : Multipulse Methods for Clean Power," Wiley-IEEE Press, Sept. 1999.

[17] Falcondes José Mendes de Seixas, Ivo Barbi, "A New 12kW Three-phase 18-Pulse High Power Factor AC-DC Converterwith Regulated Output Voltage for Rectifier Units," IEEE INTELEC International Telecommunication Energy Conference, pp.1-8, June 1999.

[18] T. B. Soeiro, T. Friedli, J. W. Kolar, "SWISS Rectifier – A Novel Three-Phase Buck-Type PFC Topology for Electric Vehicle Battery Charging," IEEE Applied Power Electronics Conference and Exposition, pp. 2617-2624, Feb. 2012.

[19] J. W. Kolar, J. Mühlethaler, "The Essence of Three-Phase PFC Rectifier Systems," Tutorial at the 7th IEEE International Power Electronics and Motion Control Conference (ECCE Asia 2012), Harbin, China, June 2012.

[20] Gui-Jia, Lixin Tang, "Current Source Inverter Based Traction Drive for EV Battery Charging Applications," IEEE VPPC Vehicle Power and Propulsion Conference, pp.1-6, Sept. 2011.

[21] P. Zavala, M. Rivera, S. Kouro, J. Rodriguez, B. Wu, V. Yaramasu, C. Baier, J. Munoz, J. Espinoza, P. Melin, "Predictive Control of a Current Source Rectifier with Imposed Sinusoidal Input Currents," IEEE IECON Industrial Electronics Society, Vienna Austria, pp. 5842-5847, Nov. 2013.

[22] I. Lizama, J. Rodríguez, B. Wu, P. Correa, M. Rivera, M. Pérez, "Predictive Control for Current Source Rectifiers Operating at Low Switching Frequency," IEEE IPMEC International Power Electronics and Motion Control, pp. 1630-1633, May 2009.

[23] Sanzhong Bai, Srdjan M. Lukic, "Unified Active Filter and Energy Storage System for an MWElectric Vehicle Charging Station," IEEE Trans. Power Electron., vol.28, no.12, pp.5793-5803, Dec. 2013.

[24] Luís Guilherme Barbosa Rolim, Diogo Rodrigues Costa, Maurício Aredes, "Analysis and Software Implementation of a Robust Synchronizing PLL Circuit Based on the pq Theory," IEEE Trans. Ind. Electron., vol.53, no.6, pp.1919-1926, Dec. 2006.

[25] José Rodríguez, Jorge Pontt, César A. Silva, Pablo Correa, Pablo Lezana, Patricio Cortés, Ulrich Ammann, "Predictive Current Control of a Voltage Source Inverter," IEEE Trans. Ind. Electron., vol.54, no.1, pp.495-503, Feb. 2007.

[26] Bruno Exposto, Helder Carneiro, Carlos Couto, João L. Afonso, "Simulations of a Current-Source Shunt Active Power Filter with Carrier- Based PWM and Periodic Sampling Modulation Techniques," EPE European Conference on Power Electronics and Applications, Birmingham - United Kingdom, pp.1-8, Aug. 2011.